Available online at www.sciencedirect.com
SCIENCE DIRECT
Polymer 46 (2005) 1139–1150
polymer
www.elsevier.com/locate/polymer

Electrophoresis of functionalized microgels: morphological insights☆

Todd Hoare, Robert Pelton*

Department of Chemical Engineering, Center for Pulp and Paper Research, McMaster University, 1280 Main Street, West Hamilton, Ont., Canada L8S 4L7

Accepted 30 September 2004
Available online 2 December 2004

Abstract

The electrophoretic mobility of thermosensitive poly(*N*-isopropylacrylamide) (PNIPAM) microgels, functionalized to contain the same bulk carboxylic acid content using acrylic acid (AA), methacrylic acid (MAA), vinylacetic acid (VAA) and acrylamide hydrolyzed in situ (H-AM), is fit to the soft particle mobility model developed by Ohshima. Good model fits were achieved for experimental mobility data as a function of both ionic strength and temperature. The model deconvolutes the underlying contributions to soft particle mobility, identifying large morphology differences between microgels with similar absolute mobility values (i.e. AA-NIPAM and VAA-NIPAM). The differences in the predicted morphologies can be correlated to the physical properties of the carboxylic acid-containing comonomers and independent light scattering data. Theoretical softness models significantly overestimate the best-fit softness of the microgels but give reasonable estimates of how the softness changes as a function of temperature. Based on simultaneous comparisons of the best-fit softness, volumetric charge density, mobility, and particle size profiles, functionalized microgels appear to deswell primarily through a consecutive core-shell mechanism.

Keywords: Electrophoresis; Functional microgels; Morphology

1. Introduction

'Smart' materials which exhibit fast, specific, and tunable responses to changes in their external environment have been the subject of increasing attention. One such material is poly(*N*-isopropylacrylamide) (PNIPAM), which can be crosslinked to produce highly monodisperse, thermosensitive sub-micron gel particles. First synthesized in our group [1], PNIPAM-based microgels deswell dramatically as the temperature is increased above the volume phase transition temperature, allowing for precise thermal tuning of the microgel volume, surface charge density, water content, and refractive index [2].

When PNIPAM-based microgels are functionalized with pH-ionizable, hydrophilic and reactive carboxylic acid groups, the 'intelligence' of the microgels can be tuned over an even wider range of environmental conditions to generate fast and targeted swelling responses to multiple external stimuli (i.e. both temperature and pH). However, to better exploit functionalized microgels for specific applications, an understanding of the functional group distribution within the three-dimensional gel matrix and the impact of this distribution on the local microgel morphology are required. Of particular interest is the local charge density and chain conformation near the microgel surface. Surface localization of functional groups has been shown in our previous work to play a key role in regulating the phase transition behavior of microgels [3]. Furthermore, the near-surface chain conformation and charge density regulate how other molecules interact with the colloidal gel and how quickly molecules can diffuse in and out of the microgel phase. This knowledge is critically important in the design of optimized microgels for applications which rely on microgel network diffusion, such as heavy metal recovery and drug delivery or uptake.

In our previous work [3,4], we discussed the synthesis of carboxylic acid-containing microgels via the free-radical

Paper presented at the 2004 Polymers in Dispersed Media Conference in Lyon, France.

* Corresponding author. Tel.: +1 905 525 9140x27045; fax: +1 905 528 5114.
E-mail addresses: hoaretr@mcmaster.ca (T. Hoare), peltonrh@mcmaster.ca (R. Pelton).

0032-3861/$ - see front matter © 2004 Elsevier Ltd. All rights reserved.
doi:10.1016/j.polymer.2004.11.055

copolymerization of four different functional monomers: acrylic acid (AA), methacrylic acid (MAA), vinylacetic acid (VAA) and acrylamide (AM), selectively hydrolyzed in situ to generate the acid groups. These four monomers differ significantly in their relative hydrophobicities and kinetic and chemical reactivities with the other gel components. AM is significantly more hydrophilic than the other monomers under the acidic conditions used in the synthesis, while AA is only slightly more hydrophilic than MAA and VAA. AM copolymerizes randomly with NIPAM [5] while AA propagates slower and MAA propagates faster than acrylamide-based monomers such as NIPAM under the acidic reaction conditions [6,7]. Furthermore, while AA, MAA, and AM all react via standard free radical propagation, VAA reacts primarily via slow chain transfer, creating a 'hairy', lightly-crosslinked surface with a high concentration of carboxy-terminated chain ends [3]. Based on these physical properties and our experimental results, we have proposed functional group distributions for each functionalized microgel: a uniform charge distribution in H-AM-NIPAM, a NIPAM-rich core/carboxylic acid-rich shell morphology in AA-NIPAM, a carboxylic acid-rich core/NIPAM-rich shell in MAA-NIPAM, and an 'extreme' core-shell microstructure in VAA-NIPAM with highly surface-localized charges.

In this paper, the electrophoretic behavior of these four carboxylic acid-functionalized microgels, all of which contain the same bulk carboxylic acid content, is analyzed to provide further evidence for the proposed microgel morphologies. Several previous studies [8–12] have shown that PNIPAM-based microgels are electrophoretically 'soft' particles in that electroosmotic flow can occur within the microgels when an external electric field is applied. A mathematical model described by Ohshima [13] for soft particles is herein applied to successfully describe the electrophoretic behavior of the functionalized microgels. Model fits to the experimental mobility versus ionic strength and temperature profiles are then used to semi-quantitatively estimate both how localized the functional groups are within the microgel and how easily substrates can penetrate into the gel. The model results are also combined with light scattering data to develop an improved picture of how phase transitions proceed in functionalized microgels.

2. Theoretical background

A theoretical treatment for the electrophoretic mobility μ of colloidal particles with a soft, ion-penetrable electrolyte shell and a hard core has been developed by Ohshima [13]. This model is based on the observation that the potential deep inside the polyelectrolyte layer is approximately equal to the Donnan potential when the surface layer is much thicker than the Debye length (i.e. $\kappa d \gg 1$). To simplify the model for practical use, two assumptions must be made: the microgel is suspended in a symmetrical electrolyte of valence v and concentration n and all charges are contained in a polyelectrolyte 'shell' with uniform charge density N. The resulting model is given in Eq. (1).

$$\mu = \frac{\varepsilon_0 \varepsilon_r}{\eta} \left(\frac{\frac{\psi_0}{\kappa_m} + \frac{\psi_{DON}}{\lambda}}{\frac{1}{\kappa_m} + \frac{1}{\lambda}} \right) f\left(\frac{d}{a}\right) + \frac{zeN}{\eta \lambda^2} \tag{1}$$

Here, ε_0 is the permittivity of a vacuum, ε_r is the relative permittivity of the suspension medium, η is the viscosity, z is the valence of the fixed ionic charges in the polyelectrolyte layer and e is the elementary charge. Ψ_0 is the potential at the boundary between the surface polyelectrolyte layer and the bulk solution and can be expressed analytically as:

$$\Psi_0 = \frac{kT}{ve} \left(\ln \left[\frac{zn}{2vn} + \left\{ \left(\frac{zN}{2vn} \right)^2 + 1 \right\}^{1/2} \right] + \frac{2vn}{zN} \left[1 - \left\{ \left(\frac{zN}{2vn} \right)^2 + 1 \right\}^{1/2} \right] \right) \tag{2}$$

k is the Boltzmann constant and T is the absolute temperature. Ψ_{DON} is the Donnan potential of the soft polyelectrolyte shell and is given by the corresponding expression:

$$\Psi_{DON} = \frac{kT}{ve} \ln \left[\frac{zN}{2vn} + \left\{ \left(\frac{zN}{2vn} \right)^2 + 1 \right\}^{1/2} \right] \tag{3}$$

κ_m is the effective Debye–Hückel parameter of the polyelectrolyte shell, accounting for charge screening due to both the free electrolyte and the fixed charges within the shell:

$$\kappa_m = \kappa \left[1 + \left(\frac{zN}{2vn} \right)^2 \right]^{1/4} \tag{4}$$

λ is the drag coefficient, related to the frictional coefficient γ retarding electrolyte flow through the polyelectrolyte shell via the expression:

$$\lambda = \left(\frac{\gamma}{\eta} \right)^{1/2} \tag{5}$$

As $\lambda \to \infty$ $(1/\lambda \to 0)$, the frictional resistance becomes infinite and fluid cannot flow through the particle (i.e. the particle becomes 'hard'). As a result, the term $1/\lambda$ is referred to as the electrophoretic softness. An increase in softness relates to a decrease in frictional resistance to electrolyte flow through the soft shell. The softness parameter is generally considered to correlate primarily to the polymer chain density in the shell and has been modeled both analytically as a cloud of homogeneously distributed spheres (Eq. (6a) [14]) and empirically (Eq. (6b) [15] and Eq. (6c) [16,17]).

$$1/\lambda = \left\{ \frac{R^2}{18} \left[3 + \frac{4}{\phi} - 3 \left(\frac{8}{\phi} - 3 \right)^{1/2} \right] \right\}^{1/2} \tag{6a}$$

$$1/\lambda = \left\{ \frac{R^2(1-\phi)^3}{45\phi^2} \right\}^{1/2} \quad (6b)$$

$$1/\lambda = \left\{ \frac{R^2(1-\phi)}{C\phi} \right\}^{1/2} \quad (6c)$$

The constant C in Eq. (6c) relates the effective diameter of a polymer blob between crosslinking points to the macroscopic diameter of the microgel.

The $f(d/a)$ term accounts for the distortion of the applied electric field within the polyelectrolyte layer according to the relative radii of the soft shell (d) and the hard core (a) of the particle and can be analytically expressed as:

$$f(d/a) = 1 + \frac{1}{2(1+d/a)} \quad (7)$$

Given that microgels do not have a strict hard core-soft shell structure, direct measurement or even estimation of the effective core radius (a) is impractical and an assumption must be made regarding the value of $f(d/a)$. Previous studies have assumed $f(d/a)=1$ (that is, $d \ll a$) [8,11] or selected a value for a based on either the fully collapsed particle size [12] or arbitrarily to best satisfy the limiting conditions of the equations [10]. However, none of these approaches can be used with a high degree of confidence; indeed, choosing a single value for $f(d/a)$ at all is impractical since the ratio d/a changes at each new temperature and electrolyte concentration tested as the highly heterogeneous 'shell' and 'core' respond differently to the changes in the microgel environment. The model results are also minimally sensitive to $f(d/a)$; fits using the lower limit assumption $f(d/a)=2/3$ can be achieved with softness and charge density values only 10–15% different than those required to fit the curves assuming $f(d/a)=1$. As shown later, such a small difference has no significant influence on the interpretation of our results. Furthermore, assuming different $f(d/a)$ values for different microgels may unreasonably bias the model results towards a particular conclusion. Consequently, we have assumed $f(d/a)=1$ for all microgels, allowing the electrophoretic behavior of the functionalized microgels to be fully described by two parameters: the electrophoretic softness $1/\lambda$ and the shell volumetric charge density N.

3. Experimental

PNIPAM-based microgels were functionalized with acrylic acid (AA), methacrylic acid (MAA), vinylacetic acid (VAA), and acrylamide (AM) using the copolymerization methods described elsewhere [3,4]. Briefly, 1.4 g NIPAM, 0.10 g *N*,*N*-methylene(bis) acrylamide (MBA), 0.05 g sodium dodecyl sulfate (SDS), 0.10 g ammonium persulfate (APS) and an amount of the functional monomer are dissolved in 160 ml water and polymerized at 70 °C for 16 h under 200 rpm stirring. The quantity of functional monomer used in each recipe is chosen such that each product microgel has the same bulk functional group content ($(5.2\pm0.2)\times10^{-4}$ mol COOH/g dry microgel), allowing direct comparisons to be made between the swelling and electrophoresis responses of these gels without corrections for differences in the bulk carboxylic acid content. The acrylamide-NIPAM copolymer microgel was subsequently hydrolyzed at 30 °C in 0.5 N sodium hydroxide for 5 days to selectively convert the acrylamide functional groups to carboxylic acid residues [4]. Non-functionalized PNIPAM microgels were also analyzed to elucidate the effect of functional group incorporation on the structure of microgels.

The electrophoretic mobility of the functionalized microgels in their fully ionized state (pH 10) was measured using a Brookhaven ZetaPlus analyzer operating in phase analysis light scattering (PALS) mode. pHydrion pH 10 carbonate buffer (Aldrich) was diluted with Milli-Q grade water to simultaneously control the pH and ionic strength of the samples. All tested suspensions had pH values of 10.0 ± 0.1. Lyophilized microgel samples were resuspended in the buffer solutions at concentrations of 50–60 ppm. The experimental ionic strength range was chosen such that the conditions $\kappa a \gg 1$ and $\kappa d \gg 1$ are met at all experimental points, as required for the model to be valid. For particles in the 100–500 nm range of those used in this study, these conditions restrict the utility of the model to measurements made in $\geq$2 mM ionic strength solutions; the model begins to significantly overestimate the experimental absolute mobility values at lower ionic strengths. A total of 10 runs (each comprised of 15 cycles) were conducted; the reported experimental uncertainties represent the standard deviation of the replicate runs.

Particle size and scattering intensity measurements were performed by light scattering using a detector angle of 90°. A Lexel 95 ion laser operating at a wavelength of 514 nm and a power of 100mW was used as the light source. Lyophilized microgels were resuspended at a concentration of 15 ppm in 0.002 M pHydrion buffers at both pH 4 and pH 10. For the particle size measurements, correlation data was analyzed using a BI-9000AT autocorrelator (Brookhaven Instruments Corp.) and the CONTIN statistical method was used to calculate the particle size distributions. At least five replicates were conducted for each sample; experimental uncertainties reported for both the particle size and the light scattering intensity data represent the standard deviation of the replicates.

4. Results

The experimental mobility profiles were fit using a method similar to that originally proposed by Ohshima [8]. While hard particle mobilities approach zero as the ionic strength is increased, soft particle mobilities instead approach a finite limiting value since the electroosmotic

flow within the polyelectrolyte shell induces particle motion independent of the value of κ_m. From Eq. (1), as the electrolyte concentration $n \to \infty$, the soft particle mobility $\mu \to zeN/(\eta\lambda^2)$. This plateau mobility at high ionic strengths can therefore be used as an initial fitting criterion for the estimation of N and λ at a given temperature. These estimates can subsequently be tuned to fit the trajectory of the mobility versus ionic strength curve and generate best-fit values of N and λ. It should be noted that the particle size of the microgels decreases by ~10–20% as the electrolyte concentration is increased from 1 to 20 mM due to osmotic deswelling effects not accounted for in the model. However, the magnitude of this deswelling is very small compared to the observed change in the electrophoretic mobility over this same ionic strength range (~1000% increase). This comparison illustrates that charge screening must be the dominant factor influencing the measured mobility values, allowing us to reasonably disregard osmotic deswelling in the quantitative analysis.

Fig. 1 shows the experimental mobility values as a function of the ionic strength of the pH 10 buffer. As shown, the Ohshima model provides excellent fits to the mobility versus ionic strength profiles of each tested microgel over the full 20–60 °C temperature range studied; indeed, all model predictions lie within one standard deviation of the corresponding measured mobilities. Experiments at 35, 45 and 55 °C have also been conducted over the full ionic strength range and give similar good fits to the model (the data is omitted from the graphs in Fig. 1 for clarity). Furthermore, a well-defined, non-zero plateau value is observed at high ionic strengths for all the microgels tested, even in the case of the non-functionalized PNIPAM microgel at 60 °C in its 'fully collapsed' state. Thus, all microgels behave as soft particles even well above their volume phase transition temperatures. However, clear differences are observed between the different microgels in terms of both the magnitude of this plateau mobility value and how the mobility changes as a function of ionic strength and temperature.

The best-fit N and λ values from the plots in Fig. 1 can subsequently be used to predict the mobility versus temperature profiles for each of the microgels. Figs. 2 and 3 show the experimental and model predictions for the μ versus T plots of each microgel at 0.002 and 0.005 M ionic strength respectively. Good fits are achieved for each of the tested microgels at all temperatures, with model predictions again lying within one standard deviation of the measured mean mobilities. The ability of the model to correctly predict both the overall magnitudes and the onset temperatures of the distinctive two-step deswelling profile of MAA-NIPAM (reflective of a sequential NIPAM-rich shell/MAA-rich core collapse) is particularly noteworthy. Good fits were also obtained at higher ionic strengths (data not shown), although the higher error-to-absolute mobility ratios observed under these conditions hinder the practical use of such data for the analysis of the gel microstructures. Particle size measurements indicate that some microaggregation occurs at high temperatures (>50 °C) in suspensions with high ionic strength (≥0.05 M), directly accounting for the larger error bars observed in the corresponding mobility measurements.

Both Figs. 2 and 3 suggest that the mobility values of the different microgels tend to converge as the temperature is increased and the microgels approach their fully collapsed states. Mobility convergence occurs at each ionic strength tested despite the six-fold difference in the microgel mobilities in the fully swollen state and the varying degrees of functional group localization in the different microgels. This suggests that the surface charge density is the key limiting factor in determining how much a given microgel may deswell; that is, deswelling becomes thermodynamically unfavorable as the surface charge density (and, by extension, surface charge–charge repulsive forces) reach a defined 'critical' value at a particular ionic strength.

The absolute volumetric charge densities (N) and electrophoretic softness values (λ) used to fit the experimental mobility values are plotted as a function of temperature in Figs. 4 and 5, respectively. Model fits for both the charge density and the electrophoretic softness of the non-functionalized NIPAM microgel compare well with previous conductometric titrations [18] and model fits [8,10] performed on microgels prepared via similar recipes with persulfate initiators. This consistency with independent experimental observations supports the validity of the assumptions we have used to fit our data.

Electrophoretic mobility measurements at pH 4 were also used in conjunction with the measured ionization-induced swelling ratios to estimate the influence of the sulfate initiator residues on the best-fit N values at pH 10. Based on this analysis, residual sulfate groups account for only 1–5% of the volumetric shell charge densities of the functionalized microgels and are therefore neglected in the quantitative mobility analysis.

The charge density results in Fig. 4 indicate that significantly different functional group distributions are present within the carboxylic acid-containing microgels. H-AM-NIPAM has a charge density only 7% higher than the non-functionalized NIPAM gel in the swollen state at low temperatures. This demands that the effective shell volume in H-AM-NIPAM is comparatively very high such that the functional groups are distributed throughout the bulk of the microgel. Such morphology is consistent with that observed in our previous work using light scattering and non-equilibrium titration [4].

Relative to H-AM-NIPAM, the low-temperature shell charge density in MAA-NIPAM is slightly (~50%) higher while both VAA-NIPAM and AA-NIPAM have dramatically higher N values (250 and 400% higher, respectively) despite the equivalent total number of functional groups in each gel. The best-fit N values for H-AM-NIPAM, MAA-NIPAM, AA-NIPAM, and NIPAM are, however, directly correlated with the measured absolute mobility values for

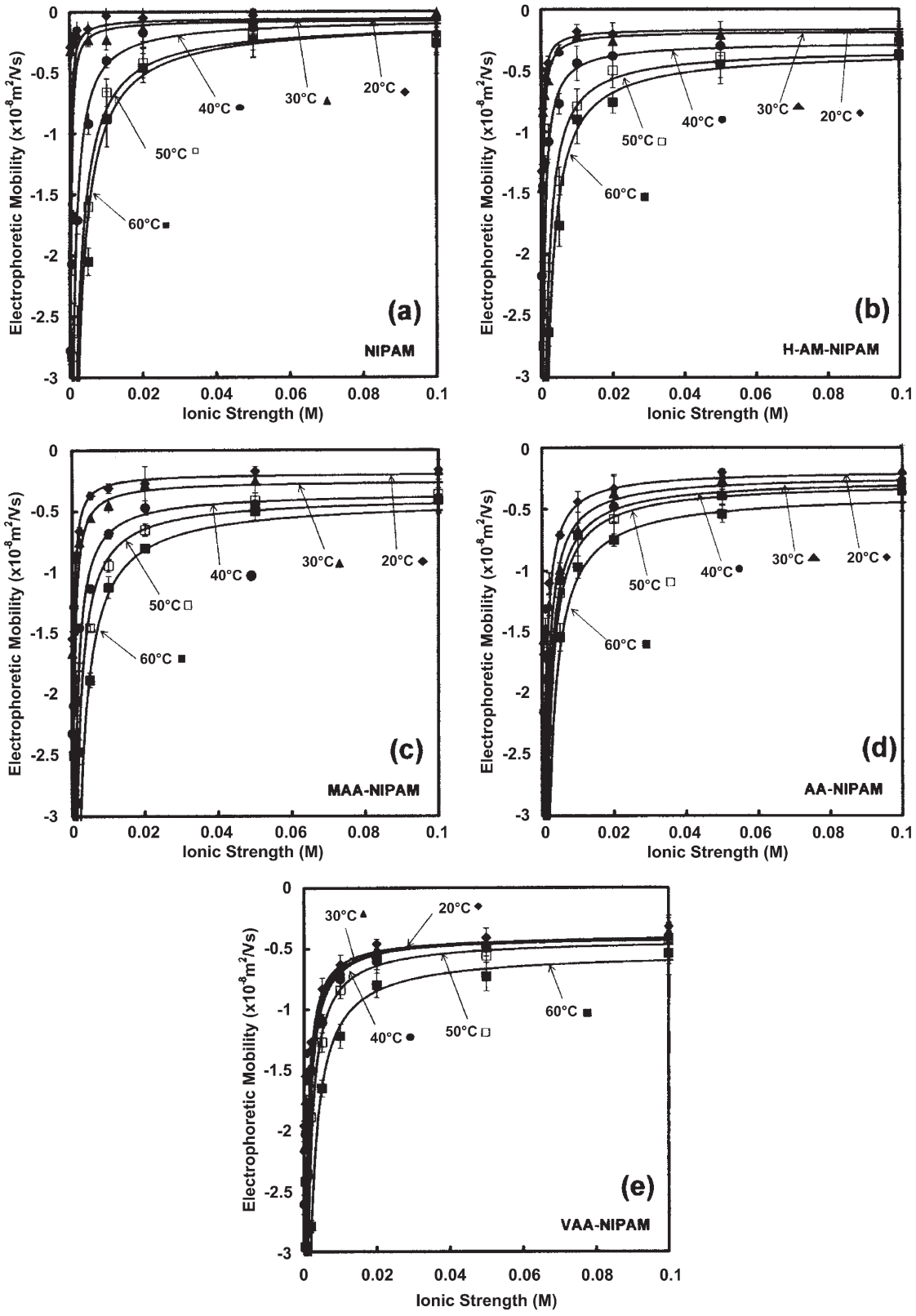

Fig. 1. Electrophoretic mobility versus ionic strength profiles for (a) NIPAM (non-functionalized); (b) H-AM-NIPAM; (c) MAA-NIPAM; (d) AA-NIPAM; (e) VAA-NIPAM in pH 10 buffer. Points are experimental data at different temperatures (according to the legend shown); solid lines are model fits at these temperatures.

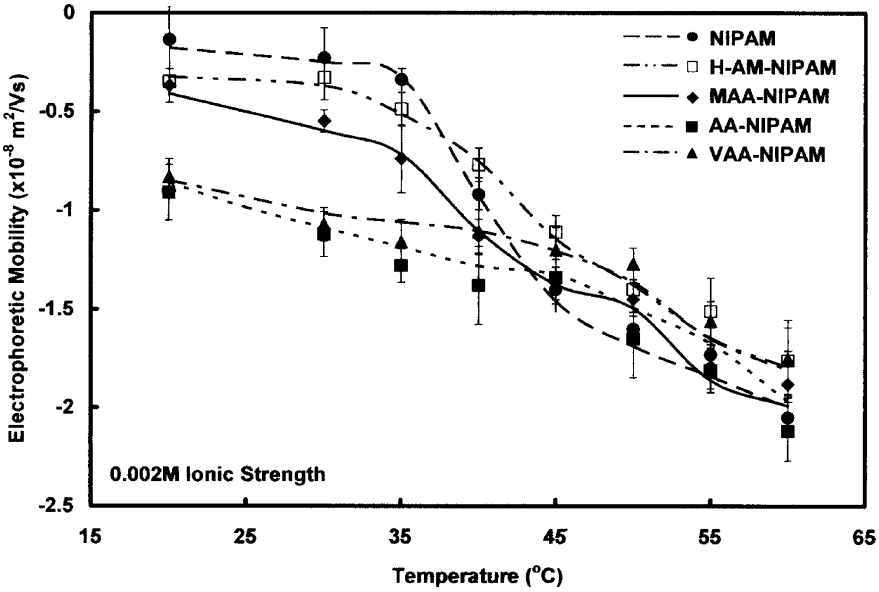

Fig. 2. Electrophoretic mobility versus temperature profiles in 0.002 M, pH 10 buffer; points are experimental data, lines are model predictions.

each microgel (Figs. 2 and 3). A general correlation also exists between the N values and the copolymerization kinetics of the comonomers; the monomers with the highest reactivity (AM and MAA) are the least surface-localized and give the lowest N microgels while the least reactive comonomers (VAA and AA) are the most shell-localized and yield the highest N microgels.

The direct correlation between the mobility, kinetics and best-fit N values for H-AM-NIPAM, MAA-NIPAM, AA-NIPAM and NIPAM suggests that the local degree of crosslinking and gel microstructure within each of the 'soft' shells is similar enough that the radial distribution of functional groups predominantly differentiates the electrophoretic behavior. However, the best-fit charge density for AA-NIPAM is 40% higher than that of VAA-NIPAM despite the fact that both VAA-NIPAM and AA-NIPAM have identical electrophoretic mobilities. Therefore, significant morphological differences must exist within the soft shells of these microgels.

Analysis of the electrophoretic softness data in Fig. 5 gives further insight into the relative morphologies of each of the microgels. As described earlier, high electrophoretic softness values imply that little frictional resistance exists toward the electroosmotic flow of electrolyte through the ion-penetrable shell of the microgel. This could occur under two circumstances: a low polymer volume fraction in the shell (i.e. the shell is highly hydrated) and a low charge content in the shell (i.e. little retardation of electrolyte flow

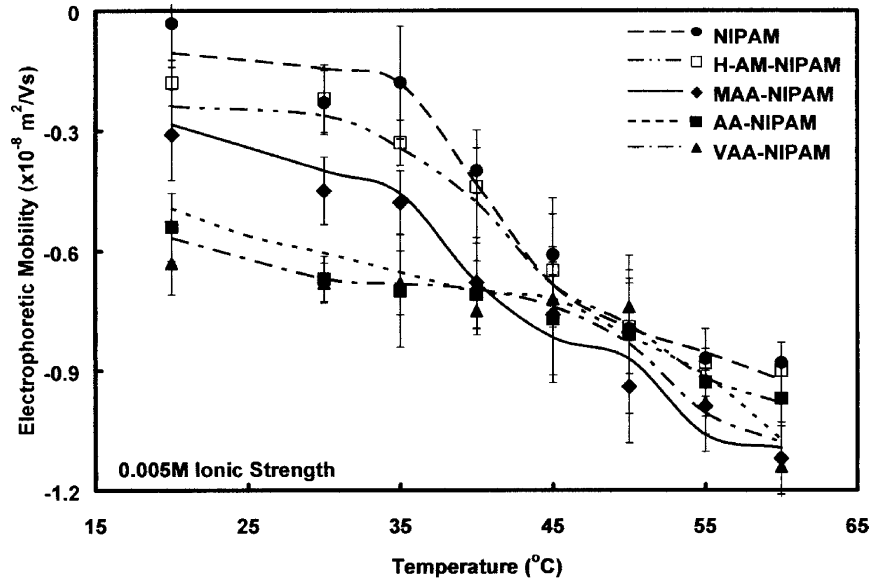

Fig. 3. Electrophoretic mobility versus temperature profiles in 0.005 M, pH 10 buffer; points are experimental data, lines are model predictions.

by ionic attractions between the flowing cations and the fixed anionic charges) [10,12]. Thus, to fully understand the factors influencing the best-fit softness values, a knowledge of the water content (i.e. the polymer chain density) within the microgels is required.

The relative degree of hydration of the microgels can be approximated by measuring the light scattering intensity of microgel suspensions, as shown in Table 1. In applying this data, it must be noted that direct quantitative correlations between scattering intensity and water content cannot be made using static light scattering since the microgels are clearly inhomogeneous; however, qualitative comparisons are practical since, on average, microgels with higher water contents have a lower refractive index gradient with the buffer and diffract less light. Table 1 also shows estimates for the microgel water contents based the 'rule of thumb' proposed by Dong and Hoffman [19], assuming 2 mol of water bind per mol of NIPAM when the microgel is in its fully collapsed state (pH 4, 60 °C). The water fraction estimates correlate well with the light scattering intensity measurements except in the case of H-AM-NIPAM. AM is significantly more hydrophilic than VAA, MAA, AA, or NIPAM under the acidic, high-temperature reaction conditions, making the assumption of only 2 mol water bound/mol NIPAM in the collapsed state unreasonable for the H-AM-NIPAM microgel.

Based on the data given in Table 1 and Fig. 5, the electrophoretic softness is not directly correlated with the water content of the microgels. MAA-NIPAM has a high electrophoretic softness while containing comparatively less water in its fully swollen state in the pH 10 buffer; on the other hand, VAA-NIPAM contains the most water per unit volume but is much less soft than MAA-NIPAM. Therefore, frictional coefficient models which consider only the polymer chain density (such as Eqs. (6(a)–(c))), are not appropriate for predicting the absolute electrophoretic softness of microgels with different functional group distributions. In fact, not only do Eqs. (6(a)–(c)) fail to predict the relative softness of the different microgels, they also predict softness values one to two orders of magnitude higher than the Ohshima model best-fit values. This observation is indicative of the key influence of the local charge density on the frictional coefficient. Indeed, direct correlations are observed between the volumetric shell charge density and the softness parameter among the functionalized microgels; microgels with higher charge densities (AA-NIPAM, VAA-NIPAM) have significantly lower softness than those with lower shell charge densities (H-AM-NIPAM, MAA-NIPAM).

As the temperature is increased, the softness decreases and N increases for all microgels, as expected over the volume phase transition. However, as shown in Figs. 4 and 5, the N and λ profiles of the different functionalized microgels are significantly different. Of particular interest, clear contrasts are observed between AA-NIPAM and VAA-NIPAM despite their identical absolute electrophoretic mobilities. VAA-NIPAM shows a distinct two-step decrease in softness from 4.8 to 3.3 nm over the measured temperature range (Fig. 5); however, no discrete volume phase transition is observed in the particle size profile (Fig. 6) and the absolute electrophoretic mobility (Fig. 2) increases continuously over this same temperature range. On the other hand, the electrophoretic softness of AA-NIPAM changes only minimally (from 2.8 nm at 20 °C to 2.4 nm at 60 °C) and in a fully continuous fashion, directly analogous to its particle size and electrophoretic mobility profiles.

Correlations are also observed between the best-fit N values and the particle size profiles in Fig. 6. In general, microgels with higher shell volumetric charge densities

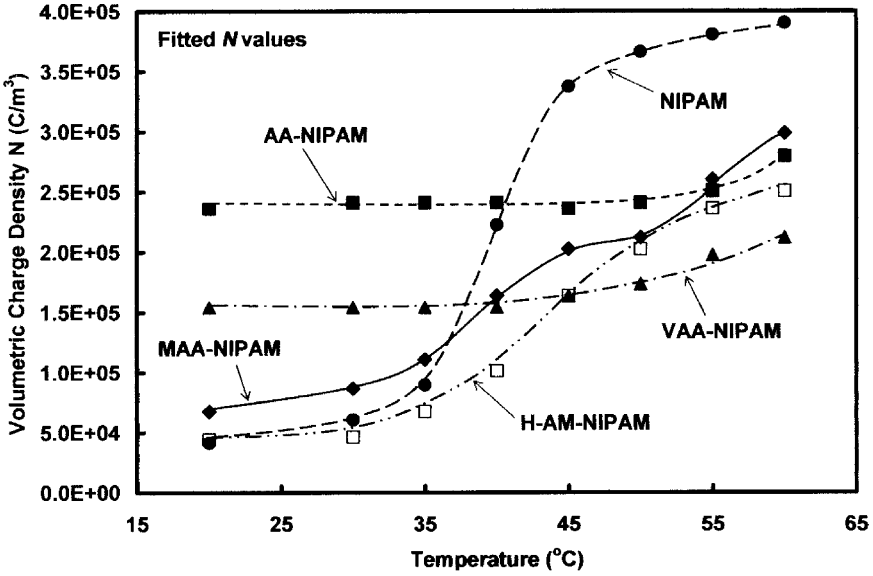

Fig. 4. Best-fit values of the volumetric charge density (N, C/m^3) for each of the tested microgels as a function of temperature at pH 10.

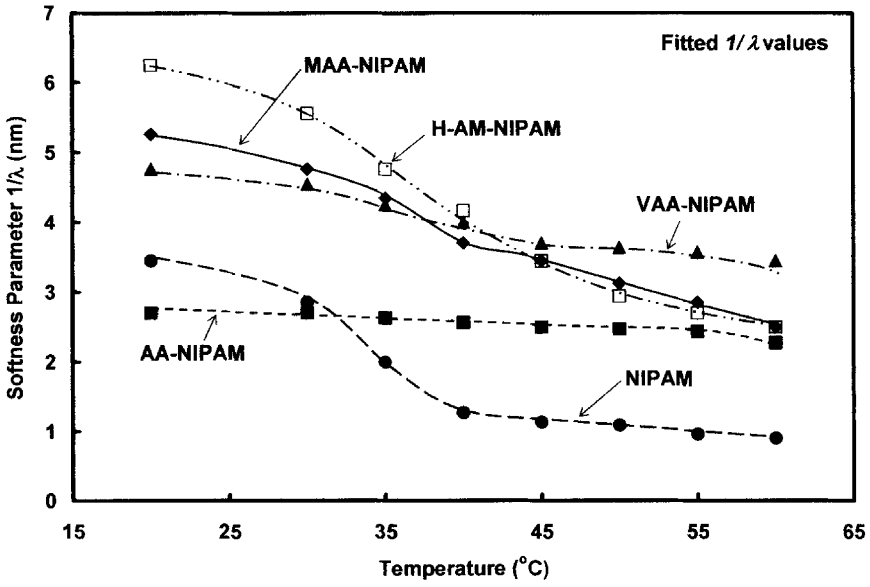

Fig. 5. Best-fit values of the electrophoretic softness ($1/\lambda$, nm) for each of the tested microgels as a function of temperature at pH 10.

have a higher volume phase transition temperature (VPTT) and deswell to a lesser degree across the volume phase transition. H-AM-NIPAM has the lowest N, shows an onset VPTT of ~31 °C, and undergoes an 85% decrease in volume across its volume phase transition; conversely, AA-NIPAM has the highest N, exhibits an onset VPTT of ~55 °C, and remains 90% swollen at the highest temperature tested. Again, however, VAA-NIPAM exhibits behavior anomalous to that of the other microgels. Both AA-NIPAM and VAA-NIPAM deswell by only 10% over the tested temperature range even though the shell volumetric charge density in VAA-NIPAM is 40% lower than in AA-NIPAM.

5. Discussion

The results from this work illustrate the utility of Ohshima's soft particle model in deconvoluting the electrophoretic mobility into its contributing components. Such information can then be used to develop a semi-quantitative picture of the relative morphologies of microgels, particularly in terms of the degree of charge localization and the effective crosslink density in the near-surface region of the gel.

In the fully swollen state, H-AM-NIPAM has the highest softness (Fig. 5), a low fixed charge density (Fig. 4) and scatters relatively weakly (Table 1). These observations are all indicative of a highly hydrated microstructure with charges delocalized throughout the bulk of the microgel, exactly the morphology one would predict based on the physical properties of acrylamide. The high relative hydrophilicity of AM encourages the formation of a more open, hydrated microstructure while the random copolymerization kinetics between AM and NIPAM should result in AM residues being distributed uniformly throughout the particle. In comparison, MAA-NIPAM has a 50% higher shell fixed charge density than H-AM-NIPAM and scatters more light, implying a denser polymer microstructure. Correspondingly, MAA is more hydrophobic than AM, resulting in the formation of a denser particle; furthermore, MAA polymerizes more quickly than NIPAM, resulting in the localization of carboxylic acid groups in the particle core. Charge localization, whether in the shell or the core, reduces the effective volume over which the majority of the charges reside, accounting for the experimentally higher N observed in MAA-NIPAM compared to H-AM-NIPAM (Fig. 4).

The power of the modeling approach for elucidating microstructure is illustrated by comparing the results for AA-NIPAM and VAA-NIPAM. At both ionic strengths shown in Figs. 2 and 3, these two microgels display statistically identical electrophoretic mobilities at least 70% higher than any of the other microgels tested in the fully

Table 1
Light scattering intensity (15 ppm microgel, 0.002 M ionic strength, pH 10) and water content predictions (as per Ref. [19]) of microgel suspensions

100 mW Laser	VAA-NIPAM	H-AM-NIPAM	AA-NIPAM	MAA-NIPAM	NIPAM
Intensity, (kcnts/s)	48.6±0.5	71.5±0.3	205.5±1.3	231.6±0.5	416.0±0.7
Predicted water content (%)	98.1	93.3	93.8	92.1	88.5

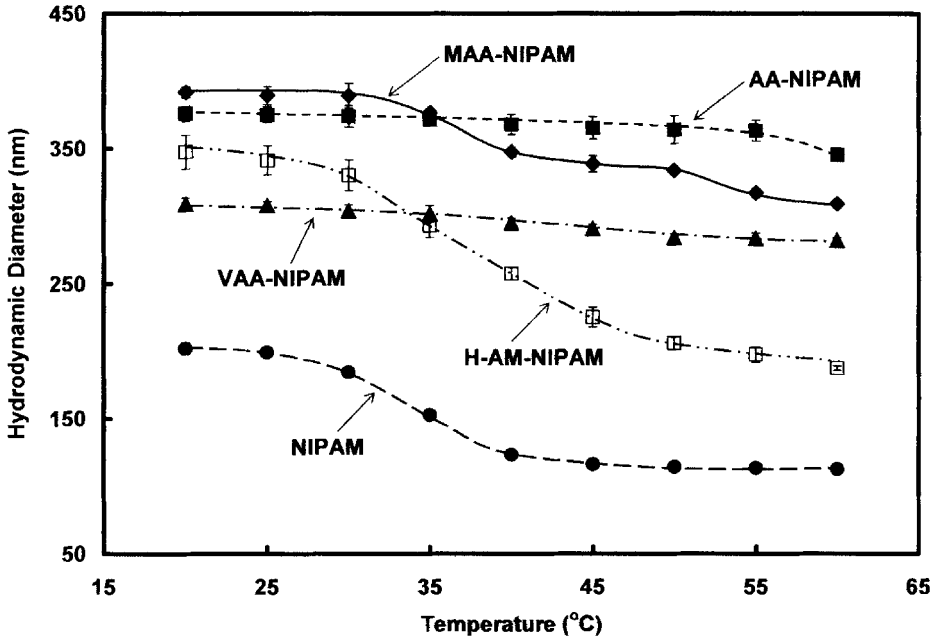

Fig. 6. Hydrodynamic diameter of the functionalized microgels as a function of temperature in 0.002 M pH 10 buffer.

swollen state. Therefore, functional groups are significantly more surface-localized in these two microgels than in the other functional microgels, in agreement with the reaction kinetics of these monomers. However, while VAA is somewhat more hydrophobic than AA under the acidic polymerization conditions, VAA-NIPAM scatters only one quarter the light of AA-NIPAM in the fully swollen state. Furthermore, VAA-NIPAM is 60% 'softer' than AA-NIPAM while having a 40% lower fixed charge density in the shell.

These results imply that VAA-NIPAM has a much thicker, more hydrated shell containing a significantly lower polymer chain density than AA-NIPAM. As a result, the fixed charges in the VAA-NIPAM network must be distributed over a much larger volume than in AA-NIPAM, accounting for the observed difference in N values. Such a 'thick shell' argument is also consistent with VAA reacting via a chain transfer pathway instead of via free radical propagation. Each chain transfer event effectively reduces the crosslink density of the microgel. As a result, the outer, charge-containing shell in VAA-NIPAM can elastically swell to a larger extent than in AA-NIPAM, accounting for the significantly lower frictional coefficient observed within the VAA-NIPAM shell. The pH swelling data in Table 2 further supports this thick shell explanation. The volume of VAA-NIPAM increases more than twice as much as that of AA-NIPAM upon ionization of the available carboxylic acid groups. Consequently, a fixed number of functional groups in the VAA-NIPAM shell must be distributed over a larger volume than the same number of functional groups in the AA-NIPAM shell.

As an aside, with the exception of the unique VAA-NIPAM microgel, the pH swelling ratios in Table 2 can be correlated directly to the best-fit N values for the microgels; the higher the volumetric shell charge density, the higher the degree of pH-induced swelling. This observation again shows the dominant role of local charge–charge repulsions in regulating the swelling behavior of functionalized microgels.

The best-fit N and λ values can also be used in conjunction with particle size data to better understand how the functionalized microgels deswell. A direct comparative analysis between variables of significantly different magnitudes and units can be achieved by reducing their values to a dimensionless scale and plotting the profiles simultaneously; a representative plot of this type is shown in Fig. 7 for H-AM-NIPAM. The '% Transition Completed' (%TC) values represent the change in variable X from its starting value (in the fully swollen state at 20 °C) to its value at temperature T, normalized by the full range of X between 20 and 60 °C (as per Eq. (8)).

$$\%\mathrm{TC} = \frac{|X_{\mathrm{T}} - X_{20\,^{\circ}\mathrm{C}}|}{|X_{60\,^{\circ}\mathrm{C}} - X_{20\,^{\circ}\mathrm{C}}|} \times 100\% \tag{8}$$

Table 2
Swelling ratio of microgels (d(pH 10)/d(pH 4)) at 0.002 M ionic strength

	VAA-NIPAM	H-AM-NIPAM	AA-NIPAM	MAA-NIPAM	NIPAM
d(pH 10)/d(pH 4)	1.57±0.06	1.06±0.03	1.24±0.04	1.12±0.03	0.99±0.02

In this work, the variable X can represent the electrophoretic mobility, hydrodynamic diameter (particle size), electrophoretic softness, or volumetric shell charge density. The %TC values therefore correspond to what percentage of the overall observed change in the variable X is complete by temperature T. Error bars represent the standard error of the mean. %TC versus temperature plots were constructed for each studied microgel; the temperatures at which %TC values of 25, 50 and 75% were achieved for each microgel and variable studied are reported in Table 3. The AA-NIPAM data estimates are included in Table 3 but are omitted from the subsequent discussion due to the large errors associated with estimating %TC values for this microgel (see the note on Table 3).

Fig. 7 and Table 3 both indicate several features which are consistent for the all the functionalized microgels examined in this work. First, the electrophoretic softness trends closely with the particle size while the mobility trends closely with the volumetric shell charge density. The latter observation is expected given how the mobility value calculated via Eq. (2) is significantly more sensitive to changes in N than to changes in λ. However, while Eqs. (6(a)–(c)) are unable to predict the absolute softness values of functionalized microgels, the observed correlation between particle size and softness suggests that the models may be able to reasonably predict how the softness changes with temperature. Using the water volume fraction predictions in Table 1 to estimate the mean polymer volume fraction in the shell, a comparison of the model-predicted and experimental softness values is given in Fig. 8. The three models give very similar predictions on a %TC scale and only the Brinkman model results (Eq. (6a)) are shown in Fig. 8 for clarity. Good qualitative and reasonable quantitative predictions of the experimental softness are achieved during and after the volume phase transition; MAA-NIPAM model and experimental data are fully correlated at %TC > 35%. However, the models consistently underestimate the softness change just prior to the volume phase transition temperature observed in Fig. 6 ($\leq$30 °C for H-AM-NIPAM, $\leq$35 °C for MAA-NIPAM, and $\leq$55 °C for AA-NIPAM).

Second, the Ohshima best-fit electrophoretic softness values consistently change at temperatures lower than those required to induce changes in either N or the particle size. A pre-VPTT softness increase is shown in comparisons of both the %TC data in Table 3 and the model and experimental softness values in Fig. 8 (note that the model predictions depend on the particle size). One possible reason for this observed behavior is microphase separation, the formation of locally-collapsed inhomogeneities in charged polyelectrolyte gels just prior to a phase transition. Microphase separation has been observed by Shibayama et al. in PNIPAM-co-AA bulk hydrogel systems [20,21] and would result in the formation of irregular, 'hard' barriers in the shell around which the electrolyte must stream. Such inhomogeneous, phase-separated domains would increase the effective frictional coefficient of the shell while only minimally influencing the particle volume, since local swelling is simultaneously induced around charged groups to maximize the entropy of the fixed charge counterions. However, further experiments are needed to definitively trace the microstructural origin of this observed softness increase.

Third, the electrophoretic mobility response consistently lags that of the particle size as the temperature is increased, by as little as 2 °C in MAA-NIPAM up to ~5 °C in H-AM-NIPAM and non-functionalized NIPAM and ~10 °C in AA-NIPAM and VAA-NIPAM. This lag has been reported previously by Daly and Saunders [11] in conjunction with non-functionalized PNIPAM microgels and, based on these results, appears to be generally applicable in functionalized

Table 3
Comparison of the transition profiles of different functionalized microgels as measured by hydrodynamic diameter (d_H) and electrophoretic mobility (μ_e) measurements and best-fit model predictions of the electrophoretic softness ($1/\lambda$) and volumetric shell charge density (N) (%TC as described in text)

%TC	Variable	VAA-NIPAM (°C)	H-AM-NIPAM (°C)	AA-NIPAM (°C)[a]	MAA-NIPAM (°C)	NIPAM (°C)
25%	$1/\lambda$	33.0	32.0	37.5	33.0	30.5
	d_H	35.0	34.0	42.5	35.5	31.5
	N	47.5	39.5	52.0	36.5	37.0
	μ_e	44.5	39.0	43.0	37.0	38.0
50%	$1/\lambda$	39.0	38.0	49.0	38.5	34.0
	d_H	40.0	39.0	56.0	39.0	34.5
	N	52.0	43.5	55.0	42.0	40.0
	μ_e	51.5	43.5	50.5	40.5	40.5
75%	$1/\lambda$	45.5	45.0	57.0	49.0	38.0
	d_H	46.5	45.5	58.0	50.5	38.0
	N	55.0	49.5	57.5	53.0	43.0
	μ_e	56.0	49.5	55.5	53.5	44.0

Temperatures are rounded to the nearest half-degree.

[a] AA-NIPAM is omitted from the discussion since only very small changes are observed in $1/\lambda$, N, μ_e and d_H over the temperature range studied; correspondingly, the calculated %TC values have large error bars ($\pm$10–20%TC) which preclude accurate estimation of the temperature at which a given %TC value is achieved.

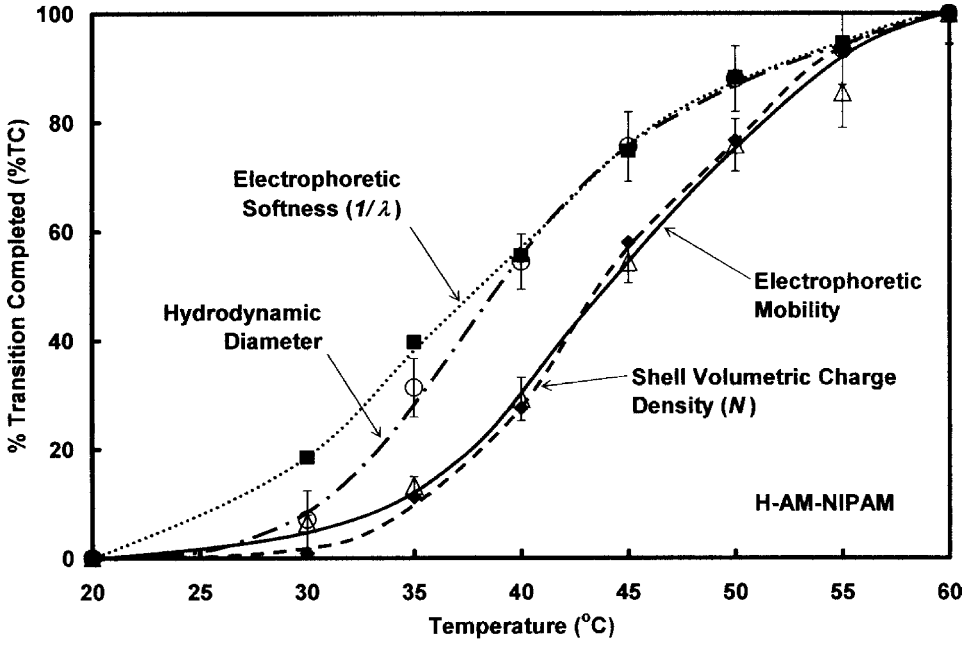

Fig. 7. Dimensionless plot of the model results (electrophoretic softness and volumetric shell charge density, filled data points) and experimental results (electrophoretic mobility and hydrodynamic diameter, unfilled data points) for H-AM-NIPAM in 0.002 M pH 10 buffer.

microgels. As has been previously suggested, the most probable explanation for this lag is the occurrence of a sequential core-shell collapse within the microgel. The segment density in the particle core is significantly higher than that in the shell, a result of the kinetic concentration of crosslinker in the centre of the particles. As a result, the core typically collapses at a lower temperature than the shell. Core collapse significantly changes the particle size but only minimally affects the mobility since the shell itself does not deswell until higher temperatures; as such, the shell simply occupies a larger fraction of the overall microgel volume such that N remains constant and d/a increases. This physically explains why the mobility response to temperature increases consistently lags that of the particle size. As the temperature is further increased, the electrostatic repulsion between the fixed charges in the shell is overcome by the increasing hydrophobic interactions and the shell undergoes a phase transition. Shell collapse induces a

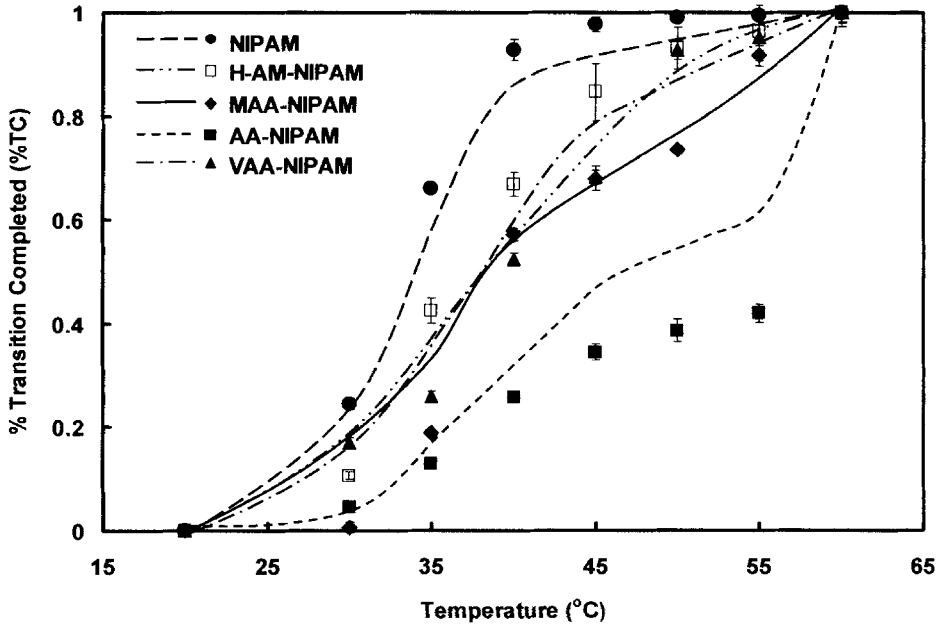

Fig. 8. Comparison between the Ohshima model best-fit softness parameter values and softness values predicted using Eq. (6a) (Brinkman model); Brinkman predictions are the data points, Ohshima best-fit values are the lines.

continued decrease in the particle size as well as the majority of the observed changes in both N and $1/\lambda$ as the shell volume decreases (higher N) and the chains become more densely packed (lower $1/\lambda$).

A comparison of the particle size and mobility responses of the different microgels tested in this study provides further support for the proposed particle morphologies. Several studies have shown that the volume phase transition temperature increases systematically with the local concentration of carboxylic acid groups in ionized microgels. In MAA-NIPAM, the localization of carboxylic acid groups in the particle core therefore effectively counteracts the transition temperature-lowering effect of the increased crosslink density in the core; consequently, the lag between the core and shell deswelling (ie. the particle size and mobility responses) is very small ($\sim$2 °C). In contrast, as functional groups become localized in the shell, the more heavily-crosslinked and lightly-functionalized core will collapse at a significantly lower temperature than the shell, thereby increasing the particle size-mobility lag to $\sim$10 °C in AA-NIPAM and VAA-NIPAM. H-AM-NIPAM and the non-functionalized NIPAM microgel, both of which are proposed to have relatively uniform volumetric charge distributions, exhibit particle size-mobility lags of $\sim$5 °C which are intermediate to that of the core-localized and shell-localized microgels. Thus, the temperature lag between the particle size and mobility responses over the volume phase transition region may be useful as a semi-quantitative parameter to compare the functional group distributions in charged microgels.

The above analysis clearly demonstrates the utility of the dimensionless %TC plots in achieving a better understanding of how different variables are correlated across the volume phase transition. Furthermore, dimensionless plots can facilitate the simultaneous comparison of independent measurements of the volume phase transition, giving insight into the underlying microstructure of the microgels and the mechanisms through which the functionalized microgels deswell.

6. Conclusions

Four major conclusions can be drawn from this work:

(1) The Ohshima soft particle mobility model can be used successfully to fit the mobility versus ionic strength and temperature profiles of carboxylic acid-functionalized microgels with significantly different functional group distributions.
(2) The model results can be used to deconvolute the respective contributions of shell charge density and electrophoretic softness to the measured mobility value, allowing for the differentiation of shell morphologies (i.e. AA-NIPAM versus VAA-NIPAM).
(3) Theoretical softness models accounting only for the polymer chain density are unable to predict the absolute Ohshima softness values. The effects of the local charge density and local inhomogeneities in increasing the frictional coefficient for electrolyte flow through the shell must also be considered. The models can, however, reasonably predict how the softness of a particular microgel changes over the volume phase transition.
(4) Volume phase transitions in functionalized microgels appear to proceed primarily through a consecutive core-shell collapse mechanism.

Overall, this work shows the utility of the soft particle electrophoresis model in acquiring morphological information not accessible through simple mobility measurements.

Acknowledgements

The authors thank the Natural Sciences and Engineering Research Council of Canada (NSERC) for financial support of this project. We also thank Dr C. Pichot for helpful discussions. Kerry Shaw and Marlene Stahel are acknowledged for their assistance with acquiring the electrophoretic mobility data.

References

[1] Pelton RH, Chibante P. Colloid Surf 1986;20:247–56.
[2] For example Pelton RH. Adv Colloid Interf Sci 2000;85:1–33. Saunders BR, Vincent B. Adv Colloid Interf Sci 1999;80:1–25.
[3] Hoare T, Pelton R. Macromolecules 2004;37:2544–50.
[4] Hoare T, Pelton R. Langmuir 2004;20:2123–33.
[5] Mumick PS, McCormick CL. Polym Eng Sci 1994;34:1419–28.
[6] Ponratnam S, Kapur SL. Makromol Chem 1977;178:1029–38.
[7] Brazel CS, Peppas NA. Macromolecules 1995;28:8016–20.
[8] Ohshima H, Makino K, Kato T, Fujimoto K, Kondo T, Kawaguchi H. J Colloid Interf Sci 1993;159:512–4.
[9] Makino K, Suzuki K, Sakurai Y, Okano T, Ohshima H. Colloid Surf A 1995;103:221–6.
[10] Rasmusson M, Vincent B, Marston N. Colloid Polym Sci 2000;278: 253–8.
[11] Daly E, Saunders BR. Phys Chem Chem Phys 2000;2:3187–93.
[12] Garcia-Salinas MJ, Romero-Cano MS, de las Nieves FJ. J Colloid Interf Sci 2001;241:280–5.
[13] Ohshima H. J Colloid Interf Sci 1994;163:474–83.
[14] Brinkman HC. Research 1948;2:190–4.
[15] Carman PC. Trans Inst Chem Eng London 1937;15:150–66.
[16] Cohen Stuart MA, Waajen FHWH, Cosgrove T, Vincent B, Crowley TL. Macromolecules 1984;17:1825–30.
[17] Fernandez-Nieves A, Fernandez-Barbero A, de las Nieves FJ, Vincent B. J Phys: Condens Matter 2000;12:3605–14.
[18] Pelton RH, Pelton HM, Morphesis A, Rowell RL. Langmuir 1989;5: 816–9.
[19] Dong L, Hoffman A. J Controlled Release 1990;30:21–31.
[20] Shibayama M, Tanaka T, Han CC. J Chem Phys 1992;97:6842–54.
[21] Shibayama M. Macromol Chem Phys 1999;199:1–30.